

Combating Noisy Labels via Dynamic Connection Masking

Xinlei Zhang¹, Fan Liu¹, Chuanyi Zhang¹, Fan Cheng¹, Yuhui Zheng¹

¹Hohai University

Abstract

Noisy labels are inevitable in real-world scenarios. Due to the strong capacity of deep neural networks to memorize corrupted labels, these noisy labels can cause significant performance degradation. Existing research on mitigating the negative effects of noisy labels has mainly focused on robust loss functions and sample selection, with comparatively limited exploration of regularization in model architecture. Inspired by the sparsity regularization used in Kolmogorov-Arnold Networks (KANs), we propose a **Dynamic Connection Masking (DCM)** mechanism for both Multi-Layer Perceptron Networks (MLPs) and KANs to enhance the robustness of classifiers against noisy labels. The mechanism can adaptively mask less important edges during training by evaluating their information-carrying capacity. Through theoretical analysis, we demonstrate its efficiency in reducing gradient error. Our approach can be seamlessly integrated into various noise-robust training methods to build more robust deep networks, including robust loss functions, sample selection strategies, and regularization techniques. Extensive experiments on both synthetic and real-world benchmarks demonstrate that our method consistently outperforms state-of-the-art (SOTA) approaches. Furthermore, we are also the first to investigate KANs as classifiers against noisy labels, revealing their superior noise robustness over MLPs in real-world noisy scenarios. Our code will soon be publicly available.

Introduction

Deep neural networks (DNNs) have achieved remarkable performance in various supervised classification (Rawat and Wang 2017; Abdou 2022; Evans, Malhotra, and Bowers 2022; Guo et al. 2023). The success largely depends on large-scale, accurately labeled data. However, acquiring high-quality labeled data remains prohibitively expensive in practice, inevitably introducing noisy labels into training datasets. Extensive studies have shown that training with these corrupted labels can cause significant performance degradation, as DNNs are prone to overfitting on corrupted labels (Zhang et al. 2021; Johnson and Khoshgoftaar 2022; Qian et al. 2023). Consequently, robust learning with noisy labels has become a critical research focus in deep learning.

Existing noise-robust training methods primarily focus on robust loss functions and sample selection strategies (Zhang and Sabuncu 2018; Ghosh, Kumar, and Sastry 2017; Song, Kim, and Lee 2019; Sun et al. 2020; Gao, Gouk, and

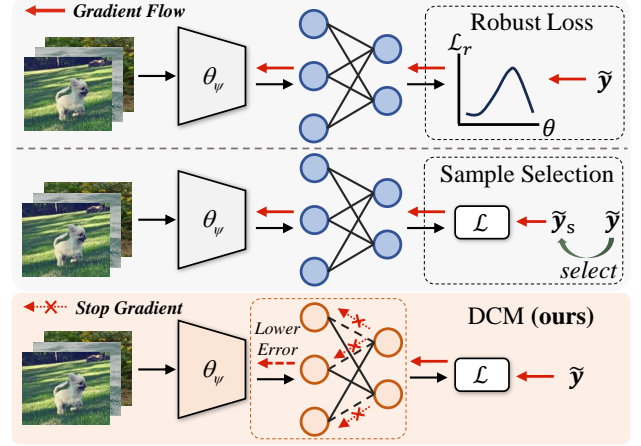


Figure 1: Comparison of different approaches for learning with noisy labels. The robust loss functions achieve noise-tolerant loss for optimization. The sample selection strategies aim to identify clean data \tilde{y}_s from noisy samples. Our dynamic connection masking (DCM) mechanism reduces gradient error by adjusting the classifier connections, allowing only important pathways for gradient backpropagation.

Hospedales 2021; Liu et al. 2024a). The former achieves risk minimization by optimizing the loss function, while the latter seeks to identify true labeled examples for training. Additionally, some regularization techniques, such as data augmentation (Zhang et al. 2017), weight decay (Krogh and Hertz 1991), can also mitigate overfitting to noisy data. However, these popular regularization methods are not tailored for noisy label scenarios and often exhibit suboptimal performance under high noise levels (Song et al. 2022). In this paper, we aim to combat noisy data through simple architectural regularization, thereby further exploring regularization techniques for noisy labels.

Recently, Kolmogorov-Arnold Networks (KANs) have emerged as a promising alternative to MLPs, demonstrating superior performance across diverse machine learning tasks (Liu et al. 2024b; Cheon 2024; Vaca-Rubio et al. 2024; Ji, Hou, and Zhang 2024). Inspired by the sparsity regularization in KANs, we propose a novel **Dynamic Connection Masking (DCM)** mechanism for both MLPs and

KANs to enhance robustness against noisy labels. Intuitively, the negative impacts of noisy labels are caused by gradient backpropagation during training. Reducing these noise-contaminated gradients would straightforwardly mitigate the adverse effects. Therefore, our DCM aims to dynamically mask less important edges by evaluating their information-carrying capacity. If an edge carries less information, it would contribute less to the prediction but have the risk of backpropagating noisy gradients. Consequently, temporarily discarding them in each training step can suppress gradient errors from noisy labels without damaging the information propagation in the network.

We present an intuitive comparison between our DCM and other noise-robust methods, as illustrated in Figure 1. Robust loss functions typically involve intricate design, which particularly requires multiple parameters to balance between noise tolerance for mislabeled samples and sufficient learning for clean samples (Wang et al. 2021; Chen et al. 2025). However, finding suitable hyperparameters for different datasets is a challenging and time-consuming task (Ding et al. 2024). Sample selection strategies rely on various heuristic criteria (*e.g.*, small loss (Jiang et al. 2018; Shen and Sanghavi 2019), predicted probability (Yi and Wu 2019; Sheng et al. 2024)), but such single criteria may fail to adapt to diverse noise conditions. Compared to these methods, which involve complex loss function designs or extra selection algorithms, our DCM serves as a simple yet effective regularization strategy. It is a novel plug-and-play module and can generalize across varying noise scenarios. The main contributions of this paper are summarized as:

- We propose a novel dynamic connection masking mechanism for both widely-used MLP-based classifiers and newly-emerged KANs for learning with noisy labels. It is plug-and-play and can be seamlessly integrated with existing noise-robust training methods for further performance enhancement.
- Theoretical analysis and experimental evidence jointly validate that our dynamic masking mechanism substantially improves noise robustness. Through adaptive edge masking during training, the approach effectively reduces the gradient error caused by noisy labels, thereby confirming significant performance improvements.
- We integrate our proposed approach into various noise-robust training methods, including robust loss functions, sample selection strategies, and regularization methods. Evaluations of both synthetic and real-world datasets demonstrate the superiority of our approach, achieving SOTA performance.
- To the best of our knowledge, this is also the first work to extend the applicability of KANs to learning from noisy labels in classification tasks. Extensive experiments demonstrate that KANs exhibit enhanced robustness to label noise over MLPs in real-world scenarios.

Related Work

Robust Loss Function. Robust loss design has been extensively studied (Qin et al. 2019; Feng et al. 2021; Szukiewicz, Good, and Dubrawski 2024; Wilton and Ye

2024). Theoretical studies have shown that certain losses like Mean Absolute Error (MAE) possess inherent noise robustness (Ghosh, Kumar, and Sastry 2017). However, empirical results indicate that MAE converges slowly (Zhang and Sabuncu 2018). Beyond this observation, the generalized cross-entropy (GCE) loss (Zhang and Sabuncu 2018) combines MAE’s robustness with CCE’s efficiency via Box-Cox transformation, allowing fast training and noise tolerance. Further studies include Active Passive Loss (APL) (Ma et al. 2020), which normalizes arbitrary losses into robust forms via active-passive combining. Furthermore, Sparse Regularization (SR) (Zhou et al. 2021b) imposes the ℓ_p -norm constraint into the loss function for robust training. Recently, the Active Negative Loss (ANL) (Ye et al. 2024) enhances APL by incorporating Normalized Negative Loss Functions, proposing a novel framework for improved performance.

Sample Selection. Unlike loss optimization, sample selection strategies aim to identify correctly labeled examples from noisy data through multi-network or multi-round learning (Yu et al. 2019; Shen and Sanghavi 2019; Patel and Sastry 2023). For instance, Co-teaching (Han et al. 2018) employs two parallel networks that cross-update using small-loss samples selected from each other, thereby reducing error accumulation. Jo-SRC (Yao et al. 2021) employs Jensen-Shannon divergence to assess prediction consistency across augmentations. DISC (Li et al. 2023) dynamically adjusts instance-specific thresholds based on its memorization momentum across training epochs, enabling adaptive noise correction. Recently, SED (Sheng et al. 2024) introduces class-balanced selection via adaptive probability thresholds, improving robustness under class-imbalanced noise.

Kolmogorov-Arnold Networks. Inspired by the Kolmogorov-Arnold representation theorem, KANs (Liu et al. 2024b) serve as a promising alternative to traditional MLPs. Unlike MLPs with fixed activation functions at nodes, KANs utilize learnable activation functions on edges. Specifically, each weight parameter is modeled as a univariate function, typically parameterized by spline functions. This architecture enhances model flexibility to better adapt to diverse data patterns (Somvanshi et al. 2024; Mohan, Wang, and Zhu 2024). Additionally, KANs can be sparsified via regularization and threshold-based pruning, removing less important neurons. While KANs have demonstrated effectiveness in various machine learning tasks, their robustness to noisy labels remains underexplored.

Method

Preliminaries

Consider a single-label classification problem with a total number of C classes. In an ideal scenario, let $D = \{(x_i, y_i)\}_{i=1}^N$ denote a clean training set, where x_i represents the i -th training image, and $y_i = \{0, 1\}^C$ indicates its one-hot encoded true label. However, acquiring a perfectly clean dataset with accurate labels y_i is often impractical. Instead, we typically have access to a noisy dataset $D_\eta = \{(x_i, \tilde{y}_i)\}_{i=1}^N$, where \tilde{y}_i represents the observed label that may differ from the true label.

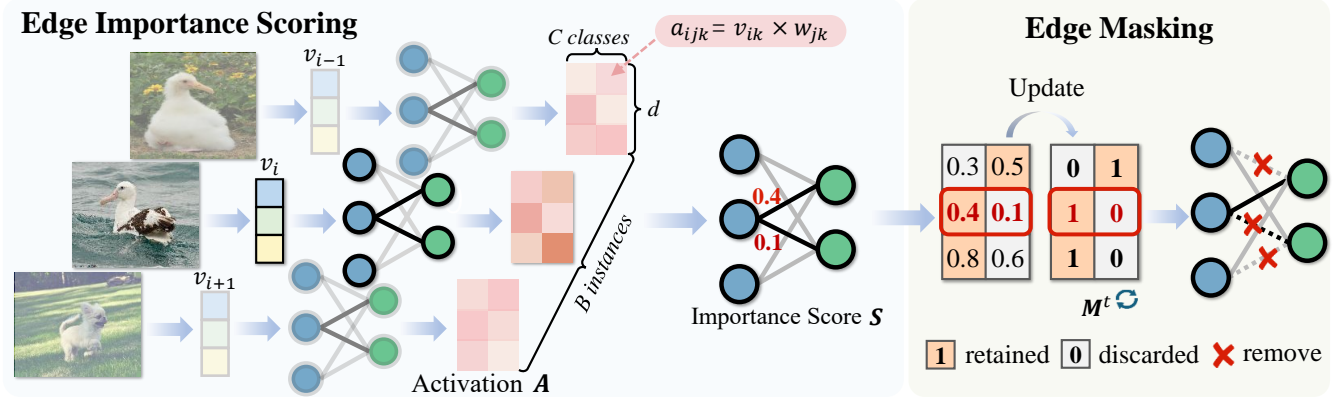


Figure 2: Overview of our dynamic connection masking mechanism. (i) We first calculate the edge activation value $\mathbf{A} \in \mathbb{R}^{B \times C \times d}$ via multiplication between the input feature v_{ik} and its corresponding edge weight w_{jk} , where B , C and d denote batch size, total class number, and the dimension of the input feature, respectively. Then, the edge importance score \mathbf{S} is obtained by measuring the standard deviation of \mathbf{A} along the batch dimension (Eq. S2). (ii) We adaptively mask edges with lower importance scores during training, dynamically adjusting the masking of connections at each timestep interval t .

A general classification model f consists of two components, which can be expressed as $f = g \circ \psi$, where a visual backbone ψ extracts feature maps $v_i = \psi(x_i) \in \mathbb{R}^d$ for the input image x_i , and a classifier g projects the input feature space to a probability distribution over the label space. The prediction probabilities are computed via the softmax function: $p_{ij} = \frac{e^{z_{ij}}}{\sum_{c=1}^C e^{z_{ic}}}$, where $z_{ij} = g_j(v_i)$ denotes the logit output of the classifier g for class j given input feature v_i . The training objective is to encourage that the global minimizer f^* obtained in the presence of label noise also serves as the global minimizer under clean label supervision (Zhang and Sabuncu 2018).

Dynamic Connection Masking

As illustrated in Figure 2, our approach encompasses two key processes: (i) edge importance scoring and (ii) edge masking. Specifically, we first compute the importance score for each connection, quantifying its ability to transmit information. Then, we dynamically mask edges with lower importance scores during training. Our approach enables the network to automatically adjust its connectivity pattern, maintaining only the most informative pathways while suppressing potentially misleading signals from noisy labels.

Edge Importance Scoring. Intuitively, the importance of an edge is associated with its ability to convey information. Specifically, edges transmitting more information inherently possess greater significance. To quantify each edge’s information-carrying capability, we adopt the standard deviation to measure the dynamic activation variability of each edge during forward propagation across different samples. A larger variance of an edge indicates that it carries more discriminative information and thus exhibits more importance.

Given the input features $\mathbf{v} \in \mathbb{R}^{B \times d}$ extracted by the visual backbone ψ , and the learnable weight matrix $\mathbf{W} \in \mathbb{R}^{C \times d}$ in a single-layer classifier, the activation value of each edge $\mathbf{A} \in \mathbb{R}^{B \times C \times d}$ is obtained by multiplying the input feature

with the corresponding edge weight:

$$a_{ijk} = v_{ik} \times w_{jk}, \quad (1)$$

where B is the batch size, $i \in \{1, \dots, B\}$, $j \in \{1, \dots, C\}$, and $k \in \{1, \dots, d\}$ represent the index of the sample, output node, and input node, respectively. Subsequently, the edge importance score $\mathbf{S} \in \mathbb{R}^{C \times d}$ is defined as the standard deviation of the edge activation value \mathbf{A} across samples:

$$s_{jk} = \sqrt{\frac{1}{B} \sum_{i=1}^B (a_{ijk} - \mu_{jk})^2}, \quad \mu_{jk} = \frac{1}{B} \sum_{i=1}^B a_{ijk}, \quad (2)$$

where μ_{jk} denotes the mean activation value of the edge between the output node j and input node k across all samples.

Our edge scoring mechanism evaluates the importance of individual edges, thereby establishing an optimized basis for dynamic edge masking.

Edge Masking. The dynamic masking mechanism adaptively adjusts the classifier connectivity using edge importance scores. Specifically, it involves dynamically updating the edge mask matrix to control which edges are retained or temporarily discarded. We introduce a hyperparameter $p \in (0, 1)$ to control the masking ratio. For each input node k , its connections are ranked in ascending order by importance scores s_{jk} , and the bottom $q = \lfloor p \times C \rfloor$ of these connections are removed, where $\lfloor \cdot \rfloor$ denotes the floor operation.

Formally, the masking edges set U_k , which contains indices of edges to be masked for each input node k :

$$U_k = \left\{ j \mid j \in \text{argsort}_j(s_{jk})_{1:q} \right\}, \quad (3)$$

where $\text{argsort}(\cdot)$ returns the edge indices j of s_{jk} sorted in ascending order. Then, the binary mask matrix $\mathbf{M} \in \mathbb{R}^{d \times C}$ is defined as:

$$m_{kj} = \begin{cases} 0, & j \in U_k \\ 1, & \text{otherwise} \end{cases}, \quad (4)$$

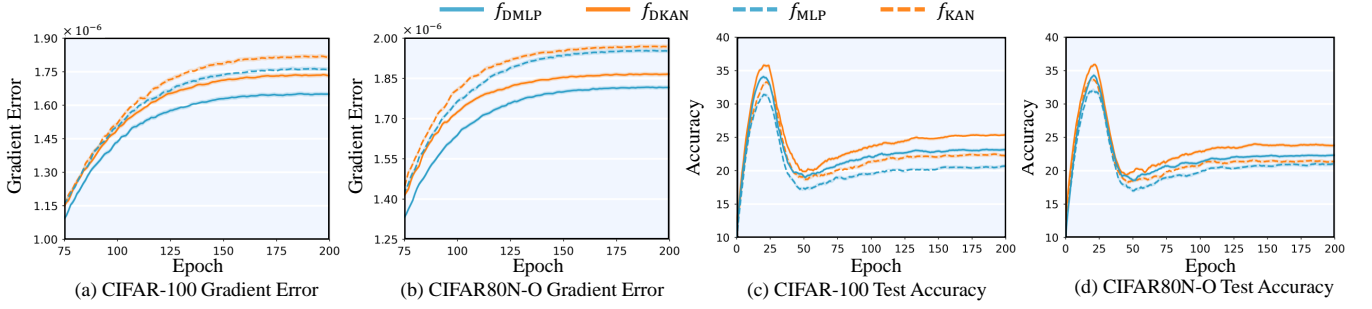


Figure 3: Comparison of gradient errors and test accuracy across various models employing different classifiers. Specifically, f_{DMLP} and f_{DKAN} denote ResNet-34 architecture with dynamic connection masking, respectively, both with a masking rate p of 0.6. While f_{MLP} and f_{KAN} represent models with standard classifiers. Figures (a) and (b) show the average L2-norm gradient errors at layer4 of the ResNet-34 backbone over training epochs on CIFAR100 and CIFAR80-NO datasets under 60% symmetric noise, respectively. Figures (c) and (d) illustrate the corresponding test accuracies obtained with different models.

where $m_{kj} = 1$ indicates that the given connection is retained, otherwise discarded. During training, the mask matrix $\mathbf{M}^{(t)}$ is dynamically updated at each timestep interval t . It allows the network to continuously evolve its connectivity pattern, facilitating adaptive masking of less important edges. After applying $\mathbf{M}^{(t)}$, the masked weight matrix is given by $\bar{\mathbf{W}}^{(t)} = \mathbf{M}^{(t)} \odot \mathbf{W}^{(t)}$, where \odot denotes element-wise multiplication. Then, the $\bar{\mathbf{W}}^{(t)}$ can be used for standard training. Benefiting from this simple masking operation, our method enables seamless integration with existing methods.

Theoretical Justification

Our DCM is implemented for both MLP and KAN classifiers, referred to as **DMLP** and **DKAN**, respectively. We provide a theoretical analysis to confirm its ability to suppress the gradient backpropagation of noisy labels, enhancing classifier robustness.

Given the clean label y_i for sample x_i , the Cross Entropy (CE) loss function is expressed as: $\mathcal{L} = -\sum_{j=1}^C y_{ij} \log p_{ij}$. When training with noisy data \tilde{y}_i , the loss becomes: $\tilde{\mathcal{L}} = -\sum_{j=1}^C \tilde{y}_{ij} \log p_{ij}$.

Then, the gradient of the visual backbone parameters θ_ψ under noisy labels is given by:

$$\sum_{i=1}^B \frac{\partial \tilde{\mathcal{L}}}{\partial \theta_\psi} = \sum_{i=1}^B (p_i - \tilde{y}_i) \cdot \frac{\partial g(v_i)}{\partial \theta_\psi}. \quad (5)$$

To quantify gradient error induced by label noise of each sample x_i , we define the gradient error ε_f^i as the L2-norm difference between noisy and clean gradients:

$$\varepsilon_f^i = \left\| \frac{\partial \tilde{\mathcal{L}}}{\partial \theta_\psi} - \frac{\partial \mathcal{L}}{\partial \theta_\psi} \right\|_2 = \left\| (y_i - \tilde{y}_i) \frac{\partial g(v_i)}{\partial \theta_\psi} \right\|_2, \quad (6)$$

where $\frac{\partial \mathcal{L}}{\partial \theta_\psi}$ represents the optimal gradient, and $\frac{\partial \tilde{\mathcal{L}}}{\partial \theta_\psi}$ denotes the noise-corrupted optimization. A smaller value of ε_f^i indicates that the gradient propagated from the noisy labels approximates the gradient derived from clean training data, demonstrating greater robustness to label noise.

Theorem 1. Given the binary edge mask matrix \mathbf{M} , the models with DCM (*i.e.*, f_{DMLP} and f_{DKAN}) demonstrate a lower gradient error than their fully-connected counterparts.

Proof. The MLP classifier with DCM is defined as:

$$g_{\text{DMLP}}(v_i) = (\mathbf{M}^T \odot \mathbf{W}) v_i + \mathbf{b}, \quad (7)$$

where \odot indicates the element-wise multiplication and \mathbf{b} represents bias vector. Thus, the gradient error ε_f becomes:

$$\begin{aligned} \varepsilon_{f_{\text{DMLP}}}^i &= \left\| \frac{\partial \tilde{\mathcal{L}}}{\partial \theta_\psi} - \frac{\partial \mathcal{L}}{\partial \theta_\psi} \right\|_2 = \left\| (y_i - \tilde{y}_i) \frac{\partial g_{\text{DMLP}}(v_i)}{\partial \theta_\psi} \right\|_2 \\ &= \left\| (y_i - \tilde{y}_i) \frac{\partial g_{\text{DMLP}}(v_i)}{\partial v_i} \frac{\partial v_i}{\partial \theta_\psi} \right\|_2 \\ &= \left\| (y_i - \tilde{y}_i) \cdot (\mathbf{M}^T \odot \mathbf{W}) \cdot \frac{\partial v_i}{\partial \theta_\psi} \right\|_2 \\ &< \left\| (y_i - \tilde{y}_i) \cdot \mathbf{W} \cdot \frac{\partial v_i}{\partial \theta_\psi} \right\|_2 \\ &= \left\| (y_i - \tilde{y}_i) \cdot \frac{\partial g_{\text{MLP}}(v_i)}{\partial v_i} \frac{\partial v_i}{\partial \theta_\psi} \right\|_2 = \varepsilon_{f_{\text{MLP}}}^i \end{aligned}$$

Similarly, we can prove $\varepsilon_{f_{\text{DKAN}}}^i < \varepsilon_{f_{\text{KAN}}}^i$ (see Appendix).

This theoretical result is also supported by our plot of the gradient error values and test accuracies on the CIFAR-100 and CIFAR80-NO with 60% symmetric noise. Figure 3 (a) and (b) illustrate the trend of gradient error $\sum_{i=1}^B \varepsilon_f^i$ with all samples at the last block (*i.e.*, layer4) of ResNet34 across training iterations. Specifically, the model performs the backpropagation using both clean and noisy labels to compute respective gradients $\frac{\partial \mathcal{L}}{\partial \theta_\psi}$ and $\frac{\partial \tilde{\mathcal{L}}}{\partial \theta_\psi}$ for recording.

Only the noisy gradients $\frac{\partial \tilde{\mathcal{L}}}{\partial \theta_\psi}$ are utilized for parameter updating. As training iterations increase, both f_{DMLP} and f_{DKAN} exhibit lower gradient errors and higher test accuracies than their fully-connected counterparts. This empirical evidence demonstrates that our approach effectively reduces the negative effects of noisy labels.

Datasets	Methods	Symmetric Noise Rate (η)				Asymmetric Noise Rate (η)	
		20%	40%	60%	80%	30%	40%
CIFAR-10	GCE	87.27 \pm 0.21	83.33 \pm 0.39	72.00 \pm 0.37	29.08 \pm 0.80	80.78 \pm 0.21	74.98 \pm 0.32
	NLNL	83.98 \pm 0.18	76.58 \pm 0.44	72.85 \pm 0.39	51.41 \pm 0.85	81.26 \pm 0.43	76.97 \pm 0.52
	SCE	88.05 \pm 0.26	82.06 \pm 0.24	66.08 \pm 0.25	30.69 \pm 0.63	79.70 \pm 0.27	78.20 \pm 0.03
	NCE+RCE	89.22 \pm 0.27	86.02 \pm 0.09	79.78 \pm 0.50	52.71 \pm 1.90	85.58 \pm 0.44	79.59 \pm 0.40
	SR	87.93 \pm 0.07	84.86 \pm 0.18	78.18 \pm 0.36	51.13 \pm 0.51	85.63 \pm 0.07	79.29 \pm 0.20
	ANL	89.72 \pm 0.04	87.28 \pm 0.02	81.12 \pm 0.30	61.27 \pm 0.55	85.52 \pm 0.24	77.63 \pm 0.31
	NCE+RCE-DMLP	89.34 \pm 0.23	86.26 \pm 0.06	80.32 \pm 0.15	56.99 \pm 1.52	86.44 \pm 0.05	80.14 \pm 0.21
	NCE+RCE-DKAN	89.60 \pm 0.24	86.49 \pm 0.16	80.25 \pm 0.21	54.39 \pm 0.48	86.45 \pm 0.23	80.63 \pm 0.15
	ANL-DMLP	89.93\pm0.13	87.45\pm0.05	81.80\pm0.20	62.98\pm0.95	86.65\pm0.23	81.05\pm0.29
	ANL-DKAN	90.16\pm0.02	87.32\pm0.09	81.69\pm0.19	63.49\pm0.09	86.54\pm0.17	81.47\pm0.30
CIFAR-100	GCE	65.24 \pm 0.56	58.94 \pm 0.50	45.18 \pm 0.93	16.18 \pm 0.46	53.99 \pm 0.29	41.49 \pm 0.79
	NLNL	46.99 \pm 0.91	30.29 \pm 1.64	16.60 \pm 0.90	11.01 \pm 2.48	42.81 \pm 1.13	35.10 \pm 0.20
	SCE	55.39 \pm 0.18	39.99 \pm 0.59	22.35 \pm 0.65	7.57 \pm 0.28	49.85 \pm 0.91	42.19 \pm 0.19
	NCE+RCE	65.31 \pm 0.07	59.48 \pm 0.56	47.12 \pm 0.62	25.80 \pm 1.12	57.82 \pm 0.41	46.79 \pm 0.96
	SR	67.51 \pm 0.29	60.70 \pm 0.25	44.95 \pm 0.65	17.35 \pm 0.13	59.09 \pm 2.10	49.51 \pm 0.59
	ANL	67.09 \pm 0.32	61.80 \pm 0.50	51.52 \pm 0.53	28.07 \pm 0.28	59.76 \pm 0.34	45.41 \pm 0.68
	NCE+RCE-DMLP	65.99 \pm 0.31	59.79 \pm 0.26	47.40 \pm 0.24	26.40 \pm 0.43	58.37 \pm 0.68	48.11 \pm 0.36
	NCE+RCE-DKAN	66.05 \pm 0.12	59.66 \pm 0.19	48.69 \pm 0.16	25.98 \pm 0.05	58.46 \pm 0.23	48.35 \pm 0.40
	ANL-DMLP	67.63\pm0.12	62.54\pm0.39	52.30\pm0.51	29.43\pm0.75	60.08\pm0.21	46.72\pm0.29
	ANL-DKAN	67.89\pm0.23	63.02\pm0.35	53.02\pm1.13	28.79\pm0.57	61.66\pm0.17	49.67\pm0.90

Table 1: Comparison with SOTA robust loss function methods on CIFAR-10 and CIFAR-100 datasets under various noise rates. Results of existing methods are mainly drawn from NCE+RCE (Ma et al. 2020). The results (mean \pm std) are reported over 3 random runs, and the top 2 best results are highlighted using boldface and underlining, respectively. The blue-highlighted regions represent the best method.

Discussion

One key motivation of our approach stems from KANs. KANs can be sparsified into smaller subnetworks by removing redundant nodes during the inference phase, which relies on a static pruning threshold. Benefiting from this sparsification paradigm, KANs can generalize well and alleviate overfitting on the training data. Building upon this property of KANs, we make three key advancements: (1) extending pruning to the training phase; (2) dynamically adjusting edge connections through importance scoring; (3) theoretically proving that such a sparse structure can mitigate the negative impact of gradient errors. These innovations enable the successful adaptation of DCM to commonly used MLP-based classifiers and emerging KANs, ultimately creating more robust models for noisy-label learning scenarios.

Experiments

We implement our DCM for both MLP and KAN classifiers, denoted as **DMLP** and **DKAN**, respectively.

Experiment Setup

Synthetically Corrupted Datasets. The CIFAR datasets are widely used in deep learning (Recht et al. 2018; Brigato and Iocchi 2021; Song and Chai 2018). The CIFAR-10 and CIFAR-100 contain 60,000 images, with 50,000 training images and 10,000 testing images. In particular, the

open-set dataset CIFAR80-NO is derived from CIFAR-100 (Krizhevsky, Hinton et al. 2009), with the last 20 categories regarded as out-of-distribution samples. The corrupted datasets are generated with both symmetric and asymmetric noise types, where the noise rate $\eta \in (0, 1)$.

Real-World Datasets. The WebVision-Mini comprises the first 50 classes from WebVision1.0 (Li et al. 2017) for training while using the validation set as the test set. Clothing1M (Xiao et al. 2015) is a large-scale, real-world noisy dataset across 14 categories of online-crawled clothing images, with 1 million training images and 10,000 test images.

Implementation Details. We evaluate our DCM by integrating it into three noise-robust training approaches: robust loss functions (NCE+RCE (Ma et al. 2020), and ANL (Ye et al. 2024)), sample selection strategies (DISC (Li et al. 2023) and SED (Sheng et al. 2024)), and a regularization method (SURE (Li et al. 2024)). When combining with robust loss functions, following (Ma et al. 2020; Zhou et al. 2021a), we use an 8-layer CNN for CIFAR-10 and ResNet-34 for CIFAR-100. For sample selection strategies and regularization methods, following (Yao et al. 2021; Sheng et al. 2024), we adopt a 7-layer CNN for CIFAR-100 and CIFAR80-NO, InceptionResNetV2 (Szegedy et al. 2017) for WebVision-Mini, and ResNet-50 (He et al. 2016) for Clothing1M. All the experiments are implemented on one NVIDIA RTX-3090 GPU. More training details are given in the Appendix.

Methods	Publication	CIFAR100			CIFAR80N-O		
		Sym-20%	Sym-80%	Asym-40%	Sym-20%	Sym-80%	Asym-40%
Co-teaching	NeurIPS 2018	43.73	15.15	28.35	60.38	16.59	42.42
Co-teaching+	ICML 2019	49.27	13.44	33.62	53.97	12.29	43.01
JoCoR	CVPR 2020	53.01	15.49	32.70	59.99	12.85	39.37
Jo-SRC	CVPR 2021	58.15	23.80	38.52	65.83	29.76	53.03
Co-LDL	TMM 2022	59.73	25.12	52.28	58.81	24.22	50.69
UNICON	CVPR 2022	55.10	31.49	49.90	54.50	36.75	51.50
SPRL	PR 2023	57.04	28.61	49.38	47.90	22.25	40.86
DISC	CVPR 2023	60.28	33.90	50.56	50.33	38.23	47.63
SED	ECCV 2024	66.50	38.15	58.29	69.10	42.57	60.87
DISC-DMLP	Ours	64.18	35.81	56.25	60.65	39.79	51.58
DISC-DKAN		66.12	38.02	56.66	61.06	41.28	54.01
SED-DMLP		<u>66.83</u>	<u>39.18</u>	59.39	69.37	44.97	<u>61.70</u>
SED-DKAN		67.16	39.49	<u>58.75</u>	<u>69.22</u>	<u>43.08</u>	62.29

Table 2: Comparison with SOTA sample selection strategies on CIFAR100 and CIFAR80N-O datasets under various noise rates. Results of existing methods are mainly drawn from SED (Sheng et al. 2024). The average test accuracy (%) is reported over the last 10 epochs, and the top 2 best results are highlighted using boldface and underlining, respectively. The blue-highlighted regions represent the best approach.

Method	Publication	Accuracy (%)
Decoupling	NeurIPS 2017	62.54
D2L	ICML 2019	62.68
MentorNet	ICML 2018	63.00
Co-teaching	NeurIPS 2018	63.58
INCV	ICML 2019	65.24
ELR+	NeurIPS 2020	77.78
GJS	NeurIPS 2021	77.99
CC	ECCV 2022	79.36
DISC	CVPR 2023	80.28
DISC-DMLP	Ours	80.80
DISC-DKAN		81.00

Table 3: Comparison with the SOTA methods on Webvision-Mini. The Top-1 validation accuracies(%) are reported, and the top 2 best results are highlighted using boldface and underlining, respectively.

Method	Publication	Accuracy (%)
Co-teaching	NeurIPS 2018	69.21
JoCoR	CVPR 2020	70.30
DMI	NeurIPS 2019	72.46
ELR+	NeurIPS 2020	74.39
GJS	NeurIPS 2021	71.64
CAL	CVPR 2021	74.17
DISC	CVPR 2023	73.72
SURE*	CVPR 2024	72.57
SURE-DMLP	Ours	73.39
DISC-DMLP		<u>74.15</u>
DISC-DKAN		74.49

Table 4: Comparison with the SOTA methods on Clothing1M. The results with * are reimplemented by us using its open-sourced code and default hyperparameters, and others are directly from the original paper.

Evaluation on Synthetic Datasets

Comparison with Robust Loss Function Methods. We integrate DCM with SOTA loss functions (NCE+RCE and ANL). Experimental results on CIFAR-10 and CIFAR-100 under both symmetric and asymmetric noise are presented in Table 1. As can be observed, our method consistently achieves significant improvements, particularly as noise levels increase. For instance, under 40% asymmetric noise on CIFAR-10, our ANL-DMLP and ANL-DKAN outperform the SOTA method (77.63% of ANL) by **3.42%** and **3.84%**, respectively. Overall, our DCM effectively enhances noise-robustness across different noise types and rates when integrating with existing robust loss functions.

Comparison with Sample Selection Strategies. We integrate DCM with SOTA sample selection strategies (DISC

and SED) and evaluate on both closed-set and open-set benchmarks. As demonstrated in Table 2, our methods exhibit superior robustness compared to their baseline counterparts. For example, our DISC-DKAN achieves 61.06% on CIFAR80N-O with 20% symmetric noise, surpassing DISC by **10.73%**. Notably, our SED-DMLP and SED-DKAN achieve the top-2 performance rankings, establishing new SOTA results on both closed-set and open-set datasets.

Evaluation on Real-world Datasets.

The experimental results on WebVision-Mini and Clothing1M are shown in Table 3 and 4, respectively. Specifically, our DISC-KAN achieves SOTA performance with accuracy of 81.00% and 74.49%, respectively. Furthermore, our method maintains an accuracy advantage of 0.82% over the

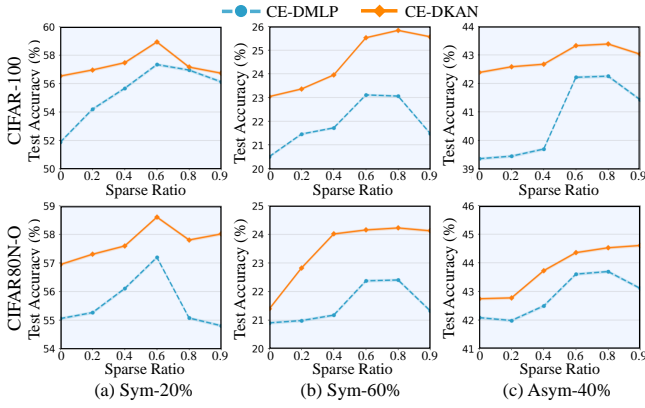


Figure 4: The effect of different masking ratios. We visualize average test accuracies over the last 10 epochs of CE under varying noise conditions on CIFAR100 and CIFAR80N-O.

Method	Masking Method	Best	Avg.
ANL	-	61.45	61.33
ANL-DMLP	Random Mask	30.37	27.23
	Edge-wise	63.91	62.92
	Node-wise	65.19	63.93
ANL-DKAN	Random Mask	61.64	61.23
	Edge-wise	62.64	61.54
	Node-wise	64.04	63.63

Table 5: Comparison of various DCM methods on CIFAR-10 with 80% symmetric noise at a fixed masking ratio of 0.6. We report both the highest (Best) and the average test accuracy (Avg.) over the last 10 epochs.

regularization method SURE on Clothing1M. Due to incompatibility between SURE’s cosine classifier and KAN’s continuous spline representations, we implement only SURE-DMLP. The results highlight that KANs exhibit superior noise robustness over MLPs in real-world scenarios.

Comprehensive evaluations on both synthetic and real-world benchmarks verify that our method offers plug-and-play compatibility with existing approaches while consistently achieving state-of-the-art performance.

Ablation Study

Masking ratio analysis. We investigate the effect of different masking ratios p on CIFAR100 and CIFAR80N-O under varying noise conditions. As illustrated in Figure 4, accuracy generally exhibits an initial increase followed by a decline as p increases under different noise conditions. An interesting phenomenon is that the optimal p tends to increase with higher noise levels and more complex noise types. It can be attributed to the fact that more severe and complex noise conditions cause greater impairment on the network, and a higher masking ratio helps mitigate overfitting to noisy data by reducing network capacity. To strike a balance between noise robustness and effective learning, we

Method	Masking Stage		Accuracy (%)	
	Training	Testing	Best	Avg.
CE-DMLP	✓		39.01	18.62
	✓	✓	40.56	18.80
CE-DKAN			41.48	17.62
	✓	✓	42.74	18.08
	✓		41.80	17.87

Table 6: Comparison with different masking stages (*i.e.*, training and testing) across different methods on CIFAR-10 with 80% symmetric noise. We report the highest (Best) and the average test accuracy (Avg.) over the last 10 epochs.

select $p = 0.6$ for all methods across different noise types.

Masking method analysis. We implement both random and edge-wise masking strategies to evaluate the efficiency of our method, where the former randomly masks connections, while the latter globally discards unimportant edges. As demonstrated in Table 5, both node-wise and edge-wise masking methods significantly outperform random masking, thus validating the effectiveness of our DCM. Furthermore, node-wise masking exhibits greater robustness compared to the edge-wise approach. This phenomenon can be attributed to the fact that edge-wise masking potentially induces more substantial alterations to network architecture, whereas node-wise masking maintains training capability for all nodes. Consequently, we employ node-wise masking, which better maintains the critical network topology while enhancing noise robustness.

Masking stage analysis. We investigate the effect of applying DCM during different stages under 80% symmetric noise on CIFAR-10. As demonstrated in Table 6, the experimental results indicate that employing DCM solely during the training phase yields better performance compared to applying it in both training and testing phases. This result demonstrates that DCM primarily serves as an effective regularization technique, hindering the model’s overfitting to noisy data. Consequently, in this study, we adopt the strategy of applying DCM exclusively during the training phase to enhance noise robustness.

Conclusion

In this study, we propose a novel dynamic connection masking (DCM) mechanism for both MLP-based classifiers and Kolmogorov-Arnold Networks (KANs) to combat noisy labels. Our DCM approach can adaptively mask unimportant edges during training while preserving the most informative pathways. Through theoretical analysis, we demonstrate that DCM effectively mitigates gradient errors propagated from noisy labels, thereby exhibiting greater noise robustness. Comprehensive experiments integrating DCM with various noise-robust training methods across synthetic and real-world datasets consistently validate the effectiveness of our approach in noisy learning scenarios.

References

- Abdou, M. A. 2022. Literature review: Efficient deep neural networks techniques for medical image analysis. *Neural Comput Appl.*, 34(8): 5791–5812.
- Brigato, L.; and Iocchi, L. 2021. A close look at deep learning with small data. In *ICPR*, 2490–2497.
- Chen, B.; Ye, Z.; Liu, Y.; Fang, X.; Lu, G.; Xie, S.; and Li, X. 2025. Towards robust semi-supervised distribution alignment against label distribution shift with noisy annotations. *IEEE Trans. Multimedia*.
- Cheon, M. 2024. Demonstrating the efficacy of kolmogorov-arnold networks in vision tasks. *arXiv:2406.14916*.
- Ding, K.; Shu, J.; Meng, D.; and Xu, Z. 2024. Improve noise tolerance of robust loss via noise-awareness. *IEEE Trans. Neural Netw. Learn. Syst.*, 36(7): 13189–13203.
- Evans, B. D.; Malhotra, G.; and Bowers, J. S. 2022. Biological convolutions improve DNN robustness to noise and generalisation. *Neural Networks*, 148: 96–110.
- Feng, L.; Shu, S.; Lin, Z.; Lv, F.; Li, L.; and An, B. 2021. Can cross entropy loss be robust to label noise? In *IJCAI*, 2206–2212.
- Gao, B.; Gouk, H.; and Hospedales, T. M. 2021. Searching for robustness: Loss learning for noisy classification tasks. In *ICCV*, 6670–6679.
- Ghosh, A.; Kumar, H.; and Sastry, P. S. 2017. Robust loss functions under label noise for deep neural networks. In *AAAI*, volume 31.
- Guo, J.; Bao, W.; Wang, J.; Ma, Y.; Gao, X.; Xiao, G.; Liu, A.; Dong, J.; Liu, X.; and Wu, W. 2023. A comprehensive evaluation framework for deep model robustness. *Pattern Recognition*, 137: 109308.
- Han, B.; Yao, Q.; Yu, X.; Niu, G.; Xu, M.; Hu, W.; Tsang, I.; and Sugiyama, M. 2018. Co-teaching: Robust training of deep neural networks with extremely noisy labels. In *NeurIPS*, 8536–8546.
- He, K.; Zhang, X.; Ren, S.; and Sun, J. 2016. Deep residual learning for image recognition. In *CVPR*, 770–778.
- Ji, T.; Hou, Y.; and Zhang, D. 2024. A comprehensive survey on kolmogorov arnold networks (kan). *arXiv:2407.11075*.
- Jiang, L.; Zhou, Z.; Leung, T.; Li, L.-J.; and Fei-Fei, L. 2018. Mentornet: Learning data-driven curriculum for very deep neural networks on corrupted labels. In *ICML*, 2304–2313.
- Johnson, J. M.; and Khoshgoftaar, T. M. 2022. A survey on classifying big data with label noise. *ACM J. Data Inf. Qual.*, 14(4): 1–43.
- Krizhevsky, A.; Hinton, G.; et al. 2009. *Learning multiple layers of features from tiny images*. Toronto, ON, Canada.
- Krogh, A.; and Hertz, J. 1991. A simple weight decay can improve generalization. In *NeurIPS*, 950–957.
- Li, W.; Wang, L.; Li, W.; Agustsson, E.; Berent, J.; Gupta, A.; Sukthankar, R.; and Van Gool, L. 2017. Webvision challenge: Visual learning and understanding with web data. *arXiv:1705.05640*.
- Li, Y.; Chen, Y.; Yu, X.; Chen, D.; and Shen, X. 2024. SURE: SURvey REcipes for building reliable and robust deep networks. In *CVPR*, 17500–17510.
- Li, Y.; Han, H.; Shan, S.; and Chen, X. 2023. Disc: Learning from noisy labels via dynamic instance-specific selection and correction. In *CVPR*, 24070–24079.
- Liu, H.; Sheng, M.; Sun, Z.; Yao, Y.; Hua, X.-S.; and Shen, H.-T. 2024a. Learning with imbalanced noisy data by preventing bias in sample selection. *IEEE Trans. Multimedia*, 26: 7426–7437.
- Liu, Z.; Wang, Y.; Vaidya, S.; Ruehle, F.; Halverson, J.; Soljačić, M.; Hou, T. Y.; and Tegmark, M. 2024b. Kan: Kolmogorov-arnold networks. *arXiv:2404.19756*.
- Ma, X.; Huang, H.; Wang, Y.; Romano, S.; Erfani, S.; and Bailey, J. 2020. Normalized loss functions for deep learning with noisy labels. In *ICML*, 6543–6553.
- Mohan, K.; Wang, H.; and Zhu, X. 2024. Kans for computer vision: An experimental study. *arXiv:2411.18224*.
- Patel, D.; and Sastry, P. 2023. Adaptive sample selection for robust learning under label noise. In *WACV*, 3932–3942.
- Qian, S.; Ying, H.; Hu, R.; Zhou, J.; Chen, J.; Chen, D. Z.; and Wu, J. 2023. Robust training of graph neural networks via noise governance. In *WSDM*, 607–615.
- Qin, Z.; Zhang, Z.; Li, Y.; and Guo, J. 2019. Making deep neural networks robust to label noise: Cross-training with a novel loss function. *IEEE Access*, 7: 130893–130902.
- Rawat, W.; and Wang, Z. 2017. Deep convolutional neural networks for image classification: A comprehensive review. *Neural Comput.*, 29(9): 2352–2449.
- Recht, B.; Roelofs, R.; Schmidt, L.; and Shankar, V. 2018. Do cifar-10 classifiers generalize to cifar-10? *arXiv preprint arXiv:1806.00451*.
- Shen, Y.; and Sanghavi, S. 2019. Learning with bad training data via iterative trimmed loss minimization. In *ICML*, 5739–5748.
- Sheng, M.; Sun, Z.; Chen, T.; Pang, S.; Wang, Y.; and Yao, Y. 2024. Foster adaptivity and balance in learning with noisy labels. In *ECCV*, 217–235.
- Somvanshi, S.; Javed, S. A.; Islam, M. M.; Pandit, D.; and Das, S. 2024. A survey on kolmogorov-arnold network. *ACM Comput. Surv.*
- Song, G.; and Chai, W. 2018. Collaborative learning for deep neural networks. In *NeurIPS*, 1837–1846.
- Song, H.; Kim, M.; and Lee, J.-G. 2019. Selfie: Refurbishing unclean samples for robust deep learning. In *ICML*, 5907–5915.
- Song, H.; Kim, M.; Park, D.; Shin, Y.; and Lee, J.-G. 2022. Learning from noisy labels with deep neural networks: A survey. *IEEE Trans. Neural Netw. Learn. Syst.*, 34(11): 8135–8153.
- Sun, Z.; Hua, X.-S.; Yao, Y.; Wei, X.-S.; Hu, G.; and Zhang, J. 2020. Crssc: salvage reusable samples from noisy data for robust learning. In *ACM MM*, 92–101.
- Szegedy, C.; Ioffe, S.; Vanhoucke, V.; and Alemi, A. 2017. Inception-v4, inception-resnet and the impact of residual connections on learning. In *AAAI*, volume 31.

Sztukiewicz, L.; Good, J. H.; and Dubrawski, A. 2024. Exploring loss design techniques for decision tree robustness to label noise. *arXiv preprint arXiv:2405.17672*.

Vaca-Rubio, C. J.; Blanco, L.; Pereira, R.; and Caus, M. 2024. Kolmogorov-arnold networks (kans) for time series analysis. *arXiv:2405.08790*.

Wang, D.-B.; Wen, Y.; Pan, L.; and Zhang, M.-L. 2021. Learning from noisy labels with complementary loss functions. In *AAAI*, volume 35, 10111–10119.

Wilton, J.; and Ye, N. 2024. Robust loss functions for training decision trees with noisy labels. In *AAAI*, volume 38, 15859–15867.

Xiao, T.; Xia, T.; Yang, Y.; Huang, C.; and Wang, X. 2015. Learning from massive noisy labeled data for image classification. In *CVPR*, 2691–2699.

Yao, Y.; Sun, Z.; Zhang, C.; Shen, F.; Wu, Q.; Zhang, J.; and Tang, Z. 2021. Jo-src: A contrastive approach for combating noisy labels. In *CVPR*, 5192–5201.

Ye, X.; Wu, Y.; Xu, Y.; Li, X.; Zhang, W.; and Chen, Y. 2024. Active negative loss: A robust framework for learning with noisy labels. *arXiv:2412.02373*.

Yi, K.; and Wu, J. 2019. Probabilistic end-to-end noise correction for learning with noisy labels. In *CVPR*, 7017–7025.

Yu, X.; Han, B.; Yao, J.; Niu, G.; Tsang, I.; and Sugiyama, M. 2019. How does disagreement help generalization against label corruption? In *ICML*, 7164–7173.

Zhang, C.; Bengio, S.; Hardt, M.; Recht, B.; and Vinyals, O. 2021. Understanding deep learning (still) requires rethinking generalization. *Commun. ACM*, 64(3): 107–115.

Zhang, H.; Cisse, M.; Dauphin, Y. N.; and Lopez-Paz, D. 2017. mixup: Beyond empirical risk minimization. *arXiv:1710.09412*.

Zhang, Z.; and Sabuncu, M. 2018. Generalized cross entropy loss for training deep neural networks with noisy labels. In *NeurIPS*, 8792–8802.

Zhou, X.; Liu, X.; Jiang, J.; Gao, X.; and Ji, X. 2021a. Asymmetric loss functions for learning with noisy labels. In *ICML*, 12846–12856.

Zhou, X.; Liu, X.; Wang, C.; Zhai, D.; Jiang, J.; and Ji, X. 2021b. Learning with noisy labels via sparse regularization. In *CVPR*, 72–81.

Appendix

Overview

This appendix provides additional details and experimental results, including detailed theoretical proof, implementation details, qualitative and quantitative results, and the algorithm description of our method.

Theoretical Justification

In this section, we provide the complete derivation of the backbone gradient $\frac{\partial \tilde{\mathcal{L}}}{\partial \theta_\psi}$ (Eq. 5 in the main paper). Additionally, we demonstrate that our **Dynamic Connection Masking** (DCM) model with KAN (f_{DKAN}) exhibits lower gradient error than the fully-connected counterpart (f_{KAN}).

Gradient Derivation of $\frac{\partial \tilde{\mathcal{L}}}{\partial \theta_\psi}$

Let p_{ij} be the predicted probability for class j of i -th sample:

$$p_{ij} = \frac{e^{z_{ij}}}{\sum_{c=1}^C e^{z_{ic}}}. \quad (\text{S1})$$

Then, the CE loss under noisy labels is:

$$\tilde{\mathcal{L}} = - \sum_{j=1}^C \tilde{y}_{ij} \log p_{ij}, \quad (\text{S2})$$

where $\tilde{y}_{ij} = 1$ if class j is assigned as the noisy label for i -th sample, and 0 otherwise. Applying the chain rule, the gradient of visual backbone parameters θ_ψ is:

$$\frac{\partial \tilde{\mathcal{L}}}{\partial \theta_\psi} = \frac{\partial \tilde{\mathcal{L}}}{\partial z_i} \cdot \frac{\partial z_i}{\partial \theta_\psi}, \quad (\text{S3})$$

where $\frac{\partial \tilde{\mathcal{L}}}{\partial z_i} = (\frac{\partial \tilde{\mathcal{L}}}{\partial z_{i1}}, \dots, \frac{\partial \tilde{\mathcal{L}}}{\partial z_{iC}})$ represents the gradient vector for the classifier output logit z_i . We first calculate the partial derivative $\frac{\partial \tilde{\mathcal{L}}}{\partial z_{ic}}$:

$$\begin{aligned} \frac{\partial \tilde{\mathcal{L}}}{\partial z_{ic}} &= - \frac{\partial}{\partial z_{ic}} \left(\sum_{j=1}^C \tilde{y}_{ij} \log p_{ij} \right) \\ &= - \sum_{j=1}^C \tilde{y}_{ij} \cdot \frac{\partial \log p_{ij}}{\partial z_{ic}} \\ &= - \sum_{j=1}^C \tilde{y}_{ij} \cdot \frac{1}{p_{ij}} \cdot \frac{\partial p_{ij}}{\partial z_{ic}}. \end{aligned} \quad (\text{S4})$$

It suffices to compute the gradient $\frac{\partial p_{ij}}{\partial z_{ic}}$. Let $\Sigma = \sum_{c=1}^C e^{z_{ic}}$, the gradient $\frac{\partial p_{ij}}{\partial z_{ic}}$ is given by:

$$\begin{aligned} \frac{\partial p_{ij}}{\partial z_{ic}} &= \frac{\partial}{\partial z_{ic}} \left(\frac{e^{z_{ij}}}{\Sigma} \right) \\ &= \frac{\frac{\partial e^{z_{ij}}}{\partial z_{ic}} \cdot \Sigma - e^{z_{ij}} \cdot \frac{\partial \Sigma}{\partial z_{ic}}}{\Sigma^2} \\ &= \frac{\frac{\partial e^{z_{ij}}}{\partial z_{ic}} \cdot \Sigma - e^{z_{ij}} \cdot e^{z_{ic}}}{\Sigma^2}, \end{aligned} \quad (\text{S5})$$

where $\frac{\partial e^{z_{ij}}}{\partial z_{ic}}$ requires case-by-case analysis:

$$\frac{\partial e^{z_{ij}}}{\partial z_{ic}} = \begin{cases} e^{z_{ic}}, & c = j \\ 0, & c \neq j \end{cases} \quad (\text{S6})$$

Then, substituting Eq. S1 and Eq. S6 into Eq. S5 obtains:

$$\frac{\partial p_{ij}}{\partial z_{ic}} = \begin{cases} p_{ic}(1 - p_{ic}), & c = j \\ -p_{ij}p_{ic}, & c \neq j \end{cases} \quad (\text{S7})$$

Thus, the partial derivative $\frac{\partial \tilde{\mathcal{L}}}{\partial z_{ic}}$ is calculated as follows:

$$\begin{aligned} \frac{\partial \tilde{\mathcal{L}}}{\partial z_{ic}} &= - \sum_{j=1}^C \tilde{y}_{ij} \cdot \frac{1}{p_{ij}} \cdot \frac{\partial p_{ij}}{\partial z_{ic}} \\ &= - \left[\tilde{y}_{ic} \cdot \frac{1}{p_{ic}} \cdot \frac{\partial p_{ic}}{\partial z_{ic}} + \sum_{j \neq c} \tilde{y}_{ij} \cdot \frac{1}{p_{ij}} \cdot \frac{\partial p_{ij}}{\partial z_{ic}} \right] \\ &= - \left[\tilde{y}_{ic} \cdot \frac{p_{ic}(1 - p_{ic})}{p_{ic}} + \sum_{j \neq c} \tilde{y}_{ij} \cdot \frac{-p_{ij} \cdot p_{ic}}{p_{ij}} \right] \\ &= - \left[\tilde{y}_{ic} \cdot (1 - p_{ic}) - \sum_{j \neq c} \tilde{y}_{ij} \cdot p_{ic} \right] \\ &= - \left[\tilde{y}_{ic} - \tilde{y}_{ic} \cdot p_{ic} - \sum_{j \neq c} \tilde{y}_{ij} \cdot p_{ic} \right] \\ &= - \left[\tilde{y}_{ic} - p_{ic} \sum_j \tilde{y}_{ij} \right] \\ &= p_{ic} \sum_j \tilde{y}_{ij} - \tilde{y}_{ic} \\ &= p_{ic} - \tilde{y}_{ic}. \end{aligned} \quad (\text{S8})$$

In vectorized form, $\frac{\partial \tilde{\mathcal{L}}}{\partial z_{ic}}$ can be expressed as:

$$\frac{\partial \tilde{\mathcal{L}}}{\partial z_i} = p_i - y_i. \quad (\text{S9})$$

Finally, the gradient of the visual backbone in Eq. S3 can be given by:

$$\begin{aligned} \frac{\partial \tilde{\mathcal{L}}}{\partial \theta_\psi} &= \frac{\partial \tilde{\mathcal{L}}}{\partial z_i} \cdot \frac{\partial z_i}{\partial \theta_\psi} \\ &= (p_i - y_i) \cdot \frac{\partial z_i}{\partial \theta_\psi} \\ &= (p_i - y_i) \cdot \frac{\partial g(v_i)}{\partial \theta_\psi}. \end{aligned} \quad (\text{S10})$$

The proof is thus complete.

Datasets	Methods	Sym-20%	Sym-80%	Asym-40%
CIFAR-10	ANL-KAN	89.99	60.22	80.83
	ANL-DKAN	90.25	63.63	81.46
CIFAR-100	SED-KAN	66.76	38.29	58.26
	SED-DKAN	67.16	39.49	58.75
CIFAR80N-O	SED-KAN	68.66	42.82	61.32
	SED-DKAN	69.22	43.08	62.29

Table 7: Comparison between standard KANs and our DKAN with different noise-robust training methods on CIFAR-10, CIFAR-100, and CIFAR80N-O datasets. The average test accuracies (%) are reported over the last 10 epochs. The blue-highlighted regions represent the best approach.

Proof for $\varepsilon_{f_{\text{DKAN}}}^i < \varepsilon_{f_{\text{KAN}}}^i$

Proof. Given the binary edge mask matrix \mathbf{M} , the KAN classifier with DCM is defined as:

$$g_{\text{DKAN}}(v_i) = \mathbf{M} \odot \phi(v_i), \quad (\text{S11})$$

where \odot indicates the element-wise multiplication, $\phi(\cdot)$ represents the trainable activation function matrix in KAN. Then, the gradient error of the model f_{DKAN} becomes:

$$\begin{aligned}
\varepsilon_{f_{\text{DKAN}}} &= \left\| \frac{\partial \tilde{\mathcal{L}}}{\partial \theta_\psi} - \frac{\partial \mathcal{L}}{\partial \theta_\psi} \right\|_2 = \left\| (y_i - \tilde{y}_i) \frac{\partial g_{\text{DKAN}}(v_i)}{\partial \theta_\psi} \right\|_2 \\
&= \left\| (y_i - \tilde{y}_i) \frac{\partial g_{\text{DKAN}}(v_i)}{\partial v_i} \frac{\partial v_i}{\partial \theta_\psi} \right\|_2 \\
&= \left\| (y_i - \tilde{y}_i) \cdot \left(\mathbf{M} \odot \frac{\partial \phi(v_i)}{\partial v_i} \right) \cdot \frac{\partial v_i}{\partial \theta_\psi} \right\|_2 \\
&< \left\| (y_i - \tilde{y}_i) \cdot \frac{\partial \phi(v_i)}{\partial v_i} \cdot \frac{\partial v_i}{\partial \theta_\psi} \right\|_2 \\
&= \left\| (y_i - \tilde{y}_i) \cdot \frac{\partial g_{\text{KAN}}}{\partial v_i} \cdot \frac{\partial v_i}{\partial \theta_\psi} \right\|_2 \\
&= \left\| (y_i - \tilde{y}_i) \frac{\partial g_{\text{KAN}}(v_i)}{\partial \theta_\psi} \right\|_2 = \varepsilon_{f_{\text{KAN}}}
\end{aligned}$$

Thus, the proof is complete.

Implementation Details

Noise generation. Following previous works, we generate noisy labels for the synthetic dataset. For symmetric noise, labels within each class are randomly flipped to incorrect labels of other classes. For asymmetric noise, labels are flipped within a specific set of related classes. For CIFAR-10, the flips are: BIRD \rightarrow BIRD, CATS \rightarrow DOG, DEER \rightarrow HORSE, and TRUCK \rightarrow AUTOMOBILE. In CIFAR-100, the 100 classes are grouped into 20 super-classes, each containing 5 sub-classes. Label flipping occurs within the same super-class circularly, with each class being flipped to the next class within the group.

Networks and training parameters. To ensure a fair and reproducible comparison, we strictly align the training parameters of our DCM approach with those of the baseline methods according to their respective original publications.

Detailed training settings are provided in Table 10, including model, epochs, batch size, learning rate (lr), optimizer, and weight decay (wd).

Quantitative Results

Comparison with Standard KANs

For a broad comparative assessment, we conduct a comprehensive comparison between our DKAN and the standard KAN when integrated with noise-robust training methodologies (ANL and SED) across multiple datasets. As demonstrated in Table 7, both ANL-DKAN and SED-DKAN consistently surpass their KAN-based counterparts under diverse noise conditions, thereby confirming the efficacy of our DCM mechanism.

Comparison of Different Masking Strategies

We further present experimental results on more different masking strategies, including masking by weight and masking of important or unimportant edges with our node-wise DCM, as shown in Table 8. It can be observed that our node-wise masking strategy, which discards unimportant edges, achieves higher accuracy compared to directly masking edges with the lowest weights. The performance improvement stems from our method’s simultaneous consideration of feature information and edge weights, thereby effectively maintaining critical connections and mitigating gradient contamination induced by noisy labels. Furthermore, masking important edges leads to a significant degradation in classification performance. This phenomenon indicates that important edges carry more information and play a crucial role in the prediction process. Consequently, removing such important edges would severely impair the model’s performance. The results also support the underlying motivation of our approach, demonstrating that selectively masking less important edges can reduce gradient errors without damaging the model’s information propagation.

Comparison of Different Masking Intervals

We evaluate different masking intervals on the CIFAR-10 dataset under symmetric noise 80% with a masking ratio of 0.6, specifically comparing the effect of masking at every

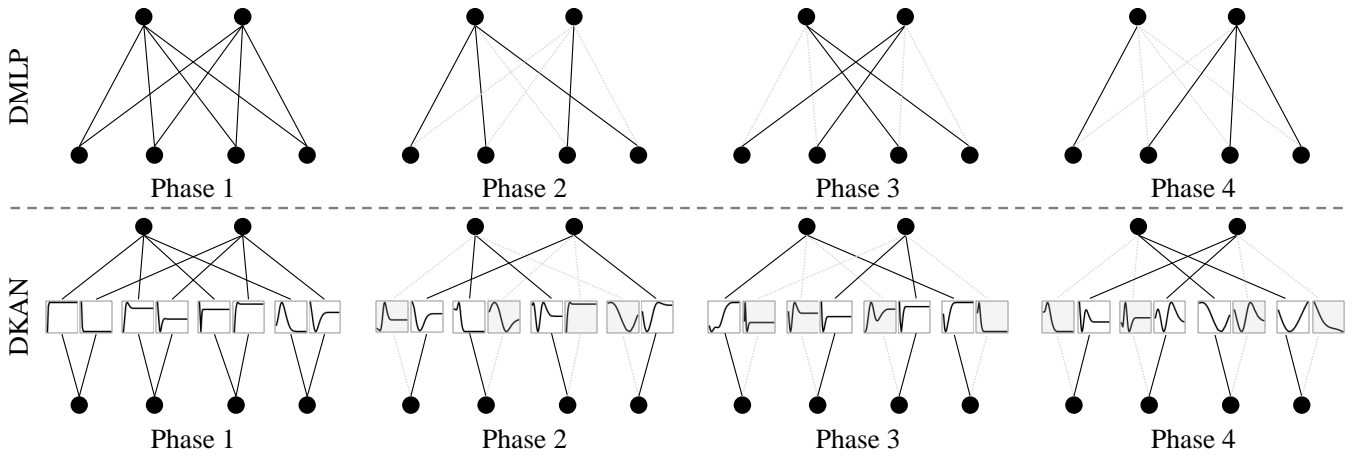


Figure 5: Visualization of DMLP and DKAN. During the training phase, the edge connection patterns dynamically adapt to optimize information flow, thereby facilitating the propagation of critical features while simultaneously improving the network’s resilience to noise.

epoch versus at every iteration during training. As demonstrated in Table 9, applying edge masking in each training iteration yields better efficiency than epoch-level masking. This experimental result suggests that more frequent edge masking enables timely updates of network connectivity patterns, thereby promoting the propagation of important information while effectively suppressing gradient backpropagation from noisy labels. Consequently, we achieve our DCM at each training step to achieve better performance.

Qualitative Results

We visualize the dynamic updating process of our approach for both the DMLP and DKAN classifiers, as illustrated in Figure 5. Beginning with a fully-connected classifier, training with our DCM can make it quite sparse. Specifically, during each training step, edges with low importance scores for individual input nodes are temporarily discarded. This adaptive masking mechanism enables the model to concentrate on more salient connections, thereby promoting the propagation of valuable information and improving overall robustness to label noise.

Algorithm Details

The process of our DCM mechanism is formally described in Algorithm 1. During the training phase, the DCM adaptively masks a subset of edges that contribute less information, as determined by their information-carrying capacity evaluated at each training step. In the testing phase, the masking mechanism is disabled, enabling the model to perform forward propagation through a standard fully connected classifier. This design ensures that the model can exploit the full spectrum of feature information, thereby potentially enhancing prediction accuracy without introducing extra computational overhead.

Method	Masking Method	Best	Avg.
ANL	-	61.45	61.33
ANL-DMLP	By Weight	63.57	62.96
	Mask Important	34.21	31.78
	Mask Unimportant	65.19	63.93
ANL-KAN	-	60.56	60.22
ANL-DKAN	Mask Important	46.38	29.17
	Mask Unimportant	64.04	63.63

Table 8: Comparison of different masking methods on CIFAR-10 with 80% symmetric noise at a fixed masking ratio of 0.6. We report both the highest (Best) and the average test accuracy (Avg.) over the last 10 epochs. The blue-highlighted regions represent the best approach.

Method	Masking Interval		Accuracy (%)	
	epoch	iteration	Best	Avg.
CE-DMLP	✓		39.01	18.62
			40.60	19.54
		✓	41.82	19.65
ANL-DMLP	✓		61.45	61.33
			64.27	63.75
		✓	65.19	63.93

Table 9: Performance comparison with different masking intervals across different methods on CIFAR-10 with 80% symmetric noise. We report both the highest (Best) and the average test accuracy (Avg.) over the last 10 epochs. The blue-highlighted regions represent the best approach.

Params	CIFAR-10	CIFAR-100 & CIFAR80N-O		Webvison-Mini	Clothing1M	
	NCE+RCE & ANL	NCE+RCE & ANL	DISC & SED	DISC	DISC	SURE
model	8-layer CNN	ResNet-34	7-layer CNN	InceptionResNetV2	ResNet-50(pt)	ResNet-50(pt)
epochs	120	200	100	100	100	100
batch size	128	128	128	32	32	32
lr	0.01	0.1	0.05	0.1	0.01	0.01
optimizer	CosineAnnealing	CosineAnnealing	CosineAnnealing	60th & 80th	50th & 80th	SAM+SWA
wd	1e-4	1e-5	5e-4	5e-4	5e-4	5e-4

Table 10: Training parameters across various datasets with different methods. The "pt" indicates the utilization of a pre-trained model, while "SAM+SWA" refers to Sharpness-Aware Minimization and Stochastic Weight Averaging optimization techniques. When integrating with different approaches, our DCM mechanism maintained parameter consistency with these methods.

Algorithm 1: Dynamic Connection Masking (DCM)

Require: X_{train} : A batch of data from the training dataset, X_{test} : A batch of data from the testing dataset, ψ : The visual backbone network, $\mathbf{W}^{(t)}$: The learnable weight matrix of MLP classifier at each step t , $\mathbf{b}^{(t)}$: The learnable bias vector of MLP classifier at each step t , $\mathbf{M}^{(t)}$: The binary mask matrix at each step t , p : The masking ratio, C : The number of classes.

Training Phase

- 1: **for** each training epoch **do**
- 2: **for** each batch of data X_{train} **do**
- 3: Extract the input features: $v \leftarrow \psi(X_{train})$;
- 4: Calculate the edge activation value: $\mathbf{A} \leftarrow v \odot \mathbf{M}^{(t)}$; *# Eq. 1 in the main paper*
- 5: Compute the edge importance score via standard deviation: $\mathbf{S} \leftarrow \text{STD}(\mathbf{A})$; *# Eq. 2 in the main paper*
- 6: **for** each input node k **do**
- 7: Sort connections by ascending importance score: $\text{sorted_indices} \leftarrow \text{argsort}(\mathbf{S}_{[:,k]})$;
- 8: Determine number of connections to mask for each input node: $q \leftarrow \lfloor p \times C \rfloor$;
- 9: Get indices of less important connections: $U_k \leftarrow \text{sorted_indices}[1 : q]$;
- 10: Generate the binary mask matrix: $\mathbf{M}^{(t)}[k, U_k] \leftarrow 0$.
- 11: **end for**
- 12: Get masked weight matrix via applying mask matrix: $\bar{\mathbf{W}}^{(t)} \leftarrow \mathbf{M}^{(t)} \odot \mathbf{W}^{(t)}$;
- 13: Compute output: $z^t \leftarrow v \cdot \bar{\mathbf{W}}^{(t)} + \mathbf{b}^{(t)}$;
- 14: Compute loss and update model parameters via backpropagation.
- 15: **end for**
- 16: **end for**

Testing Phase

- 17: Extract the input features: $v \leftarrow \psi(X_{test})$;
- 18: Remove mask for testing: $z \leftarrow v \cdot \mathbf{W}^T + \mathbf{b}$;
- 19: Compute the test accuracy.
